

Band Offset Characterization of the Atomic Layer Deposited Aluminum Oxide on m-Plane Indium Nitride

YE JIA,^{1,5} JOSHUA S. WALLACE,² YUELING QIN,³
JOSEPH A. GARDELLA JR.,² AMIR M. DABIRAN,⁴
and UTTAM SINGISETTI¹

1.—Electrical Engineering Department, University at Buffalo, Buffalo, NY 14260, USA. 2.—Chemistry Department, University at Buffalo, Buffalo, NY 14260, USA. 3.—Integrated Nanostructured Systems Initiative, University at Buffalo, Buffalo, NY 14260, USA. 4.—SVT Associates, Eden Prairie, MN 55344, USA. 5.—e-mail: yejia@buffalo.edu

In this letter, we report the band offset characterization of the atomic layer deposited aluminum oxide on non-polar m-plane indium nitride grown by plasma-assisted molecular beam epitaxy by using x-ray photoelectron spectroscopy. The valence band offset between aluminum oxide and m-plane indium nitride was determined to be 2.83 eV. The Fermi level of indium nitride was 0.63 eV above valence band maximum, indicated a reduced band bending in comparison to polar indium nitride. The band gap of aluminum oxide was found to be to 6.7 eV, which gave a conduction band offset of 3.17 eV.

Key words: m-Plane indium nitride, band offset, x-ray photoelectron spectroscopy

Indium nitride (InN) is a promising III-N semiconductor with potential applications in both optoelectronics and electronics. Due to its narrow gap (0.7 eV)^{1–4} and the ability to form alloys with GaN and AlN, it has the potential to extend III-N optoelectronic devices into the near infra-red.^{1–3} On the other hand, it also holds promise for high-speed electronics due to the large electron velocities⁵ enabled by its low effective mass. Although high electron velocities have been confirmed experimentally,⁶ serious challenges exist for real device applications. These challenges include high density of dislocations within the epitaxial InN film which lead to high background doping densities,⁷ large surface electron accumulation,^{8–10} and the difficulty of *p*-type doping.^{10,11} It has been shown that the Fermi level (E_F) at the InN surface is at ~ 1.8 eV above valence band maximum.^{12,13} Considering the small band gap, the Fermi level is deeply pinned inside the conduction band. Consequently, at the surface, it has extreme downward band bending, leading to a high carrier concentration (i.e., surface

electron accumulation). The high concentration of electrons impedes the field effect modulation of the bulk electrons in a FET structure.¹⁴ The electron accumulation layer also makes it challenging to use the conventional methods of determining bulk carrier transport properties in *p*-type doped InN.^{10,11} There have been a number of reports of partial unpinning of the InN surface after careful surface treatments and vacuum annealing,^{15–17} however, FET devices have not been demonstrated.

The deep Fermi level pinning has been attributed to the intrinsic surface properties of the polar InN surface^{18–20} in addition to external effects. Density functional theory studies have indicated that the non-polar (m-plane and a-plane) InN surfaces have reduced band bending.^{19,20} The reduced band bending in the non-polar InN surfaces have been reported *in situ* cleaved surfaces²¹ and also in InN nanowires.²² The *p*-type doping and *p*-channel devices have also been reported in nanowires.^{23,24} In addition, the non-polar and semi-polar III-Ns have distinct advantages for light emitting diodes (LEDs) and lasers due to the absence of polarization fields that separate electron and hole wave functions in polar films.²⁵

Additionally, high quality dielectrics on InN are necessary to realize InN devices. The understanding

of interfacial properties between dielectrics and InN is essential for device applications. Al_2O_3 is an excellent material for gate dielectrics, because it has a large dielectric constant (~ 8),²⁶ providing higher breakdown voltage and superior insulating properties. However, there are very few reports on the characterization of interfacial properties between non-polar InN and Al_2O_3 . In this letter, we investigate the band alignment of atomic layer deposited (ALD) Al_2O_3 on m-plane InN by using x-ray photoelectron spectroscopy (XPS).

The non-polar m-plane InN film (500 nm) was grown by plasma-assisted molecular beam epitaxy (PA-MBE) on m-plane GaN substrates at growth temperatures of 350°C with a 100 nm GaN buffer layer grown at 720°C. To avoid indium metal droplets on the surface, the indium to nitrogen ratio was set to be about 1:1. For band alignment studies, Al_2O_3 films were deposited by thermal ALD at 300°C in a Cambridge Nano Tech S100 system using trimethylaluminum (TMA) and water (H_2O).

Figure 1 shows the reflection high energy electron diffraction (RHEED) image of the grown InN films. The clean and sharp periodic diffraction spots implied good quality InN film. Figure 2 shows the x-ray diffraction (XRD) spectrum of InN/GaN. The XRD spectrum was taken from bare m-plane InN after growth. XRD spectrum showed that the peak of $(1\bar{1}00)$ InN was completely separated from $(1\bar{1}00)$ GaN, indicating a relaxed InN film.²⁷ In addition to the two $(1\bar{1}00)$ peaks, (0002) GaN and (0002) InN were also observed from the XRD spectrum, which suggests that some c-plane domains exist in the film.²⁸

Using Bragg's law of diffraction:

$$2\Lambda \sin \theta = n\lambda,$$

where the Λ is the distance between two adjacent crystal planes, θ is the diffraction angle, n is a positive integer, and λ is the incident wavelength. The lattice constants of InN and GaN were calculated to be: a (InN) = 3.55 Å, c (InN) = 5.69 Å, a (GaN) = 3.19 Å, and c (GaN) = 5.16 Å, which were in good agreement with reported values.^{3,29}

Surface morphology was characterized by scanning electron microscopy (SEM) and atomic force microscopy (AFM). Figure 3a and b show the SEM and AFM images of bare InN. We observed slate-like morphology, indicating a m-plane surface.^{30,31} The root mean square (RMS) roughness was determined to be ~ 25 nm from AFM, which was very rough. Figure 4a and b show the cross section transmission electron microscopy (TEM) at the GaN/InN interface and the InN/ Al_2O_3 interface. In Fig. 4a, it can be seen that the density of dislocations inside InN epitaxial film was very high because of the lattice mismatch at the GaN/InN interface, which is shown in the inset of Fig. 4a. In contrast, in Fig. 4b, the interface between Al_2O_3 and InN was pretty clean, and there was no significant interfacial layer. In order to characterize the lattice

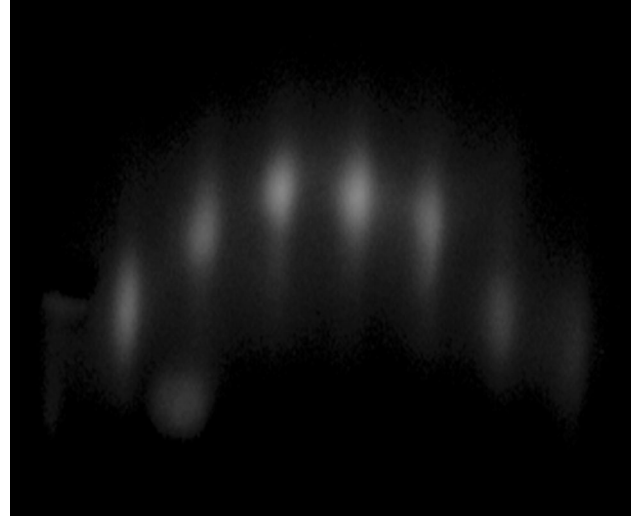


Fig. 1. RHEED image obtained from bare InN.

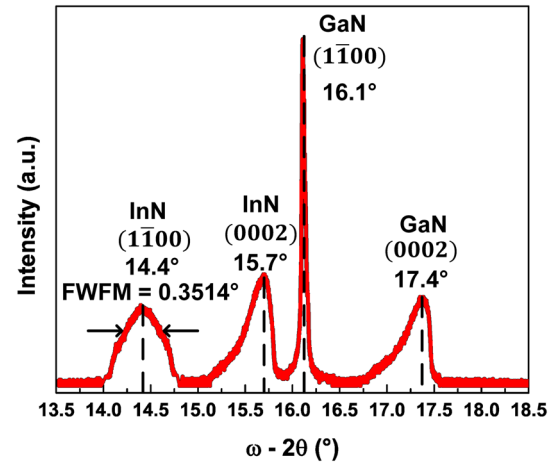


Fig. 2. XRD spectrum of GaN/InN. The lattice constants of InN were calculated to be 3.55 Å in the basal plane and 5.69 Å in the c-axis direction (color on line).

mismatch at the GaN/InN interface, the TEM diffraction patterns near the interface were acquired as shown in Fig. 5. The direction of the incident electron was in the $[0001]$ or $[000\bar{1}]$ direction. In Fig. 5, both InN and GaN lattice diffraction patterns are presented. Since the growth direction was in the $[1\bar{1}00]$ direction, so the lattice mismatch should be in the $[11\bar{2}0]$ direction. According to the TEM diffraction equation:

$$R = \frac{\Lambda L}{\lambda}, \quad (1)$$

where R is the distance between two transmitted beam spots, λL is the camera constant, and Λ is the lattice spacing. The distance (R) between two spots in the $[11\bar{2}0]$ direction for GaN and InN was found to be 6.4/nm and 5.8/nm, respectively. The lattice mismatch, $\Delta\Lambda$, can be found by:

Band Offset Characterization of the Atomic Layer Deposited Aluminum Oxide on m-Plane Indium Nitride

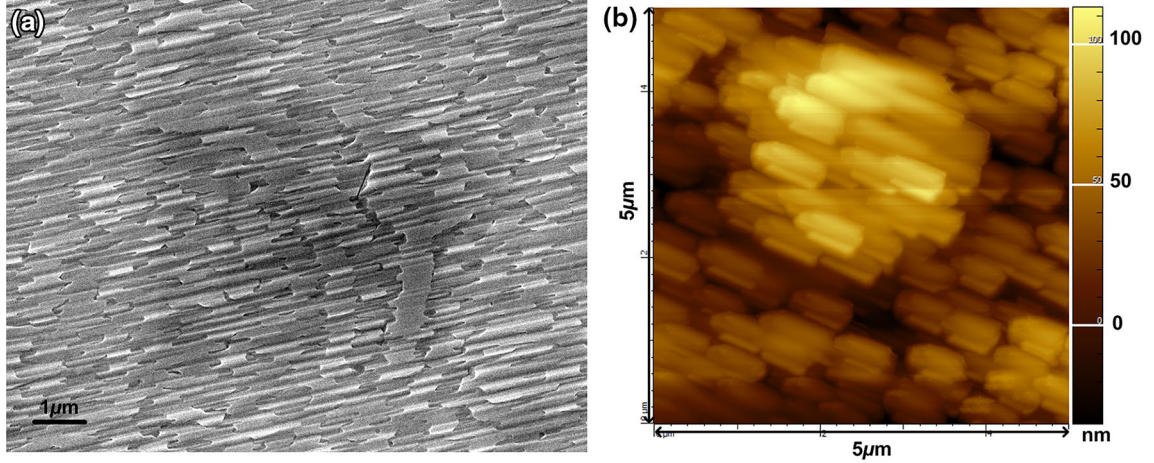


Fig. 3. (a) SEM and (b) AFM images of bare InN surface. The RMS roughness was found to be 25 nm from AFM.

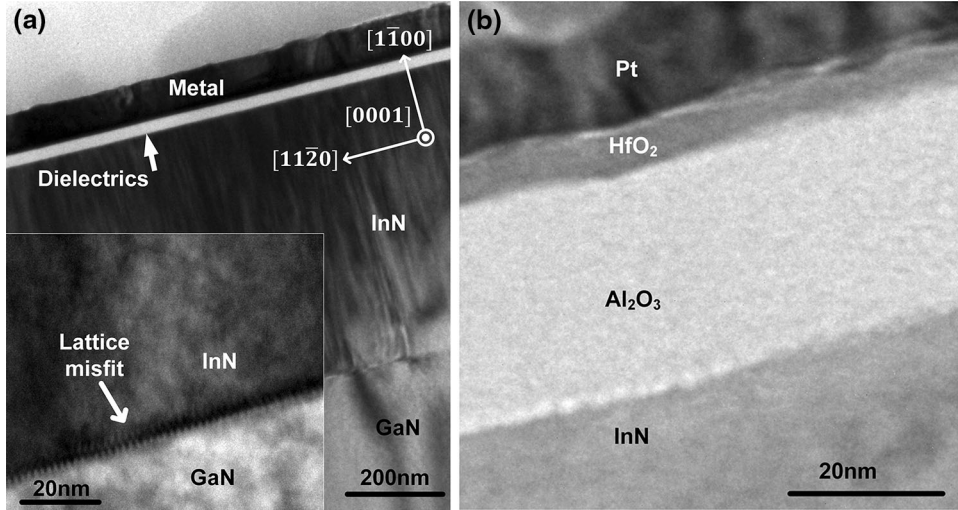


Fig. 4. Cross section transmission electron microscopy (TEM) images at (a) GaN/InN interface and (b) InN/Al₂O₃ interface. The inset of (a) shows the lattice misfit at the GaN/InN interface.

$$\Delta\Lambda = \frac{\Lambda_f - \Lambda_s}{\Lambda_s} \times 100\%, \quad (2)$$

where Λ_f , Λ_s denote the inter-planar distance of the epitaxial film and the substrate, respectively. The lattice mismatch was determined to be 10.46%, which was close to the reported value.³²

The band alignment between Al₂O₃ and InN was characterized by XPS. The XPS spectra were obtained using a Physical Electronic PHI VersaProbe 5000 equipped with a hemispherical energy analyzer. A monochromatic Al K α (1486.6 eV) was operated at 25.3 W and 15 kV. High resolution spectra were acquired by operating the energy of the analyzer at a pass energy of 11.75 eV. The energy resolution was 0.025 eV. The acquisition was performed under an ultrahigh vacuum environment (operating pressure $< 4.0 \times 10^{-6}$ Pa, background

pressure $< 1 \times 10^{-6}$ Pa). Dual charge neutralization was utilized to reduce the effects of charging on the acquired signal. Additionally, binding energies were calibrated by setting the CH_x peak in the C 1s envelope at 284.8 eV to correct for charging effects.^{33,34} However, the charging effects do not affect the band offset characterization.

The valence band offset was extracted by the method given by Kraut et al.³⁵:

$$\Delta E_v = \left(E_{\text{Al}_2\text{O}_3/\text{InN}}^{\text{Al}2p} - E_{\text{Al}_2\text{O}_3/\text{InN}}^{\text{In}3d_{5/2}} \right) + \left(E_{\text{InN}}^{\text{In}3d_{5/2}} - E_{\text{InN}}^{\text{VBM}} \right) - \left(E_{\text{Al}_2\text{O}_3}^{\text{Al}2p} - E_{\text{Al}_2\text{O}_3}^{\text{VBM}} \right), \quad (3)$$

where the superscripts indicate the XPS core level peaks and the subscripts indicate the samples. Here, we analyzed XPS spectra from three different samples: 40 nm Al₂O₃ on Si, bare InN, and ~ 2 nm

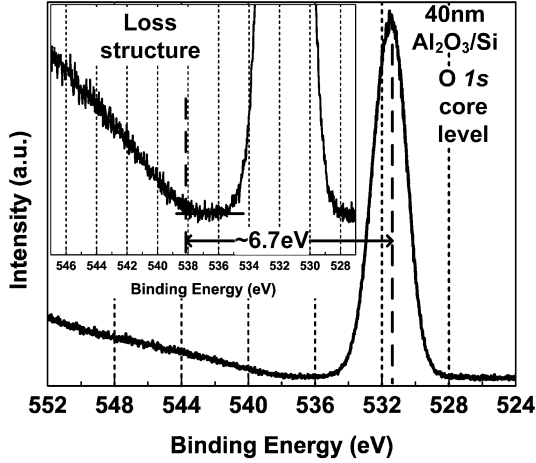


Fig. 7. O 1s peaks obtained from 40 nm $\text{Al}_2\text{O}_3/\text{Si}$ to determine the bandgap of Al_2O_3 . The inset shows the corresponding loss structure. The bandgap of Al_2O_3 was found to be 6.7 eV.

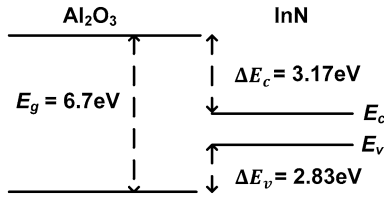


Fig. 8. Band diagram of the $\text{Al}_2\text{O}_3/\text{InN}$ heterostructure.

From XPS profiles, the $(E_{\text{Al}_2\text{O}_3}^{\text{Al}2p} - E_{\text{Al}_2\text{O}_3}^{\text{VBM}})$, $(E_{\text{InN}}^{\text{In}3d_{5/2}} - E_{\text{InN}}^{\text{VBM}})$, and $(E_{\text{Al}_2\text{O}_3/\text{InN}}^{\text{Al}2p} - E_{\text{Al}_2\text{O}_3/\text{InN}}^{\text{In}3d_{5/2}})$ were calculated to be 71.13 eV, 442.79 eV, and -368.83 eV, respectively, which gave a valence band offset (ΔE_v) of 2.83 eV. Figure 7 shows the core level and loss structure of O 1s on 40 nm $\text{Al}_2\text{O}_3/\text{Si}$. The loss structure of O 1s was used to determine the band gap of Al_2O_3 . The band gap for the insulator can be determined from the onset energy of the loss energy spectrum.^{34,40,44,45} Therefore, the band gap of Al_2O_3 was found to be ~ 6.7 eV, which was in good agreement with the reported value.^{34,46} The conduction band offset was found by:

$$\Delta E_c = \Delta E_g - \Delta E_v, \quad (4)$$

where ΔE_g is the band gap difference between Al_2O_3 and InN and ΔE_v is the valence band offset. Taking the band gap difference to be 6.0 eV, a conduction band offset of 3.17 eV was calculated. Assuming the electron affinity energies of Al_2O_3 and InN to be 2.58 eV⁴⁶ and 5.8 eV,²⁰ a conduction band offset of 3.22 eV and a valence band offset of 2.78 eV were calculated, which were in good agreement with our measurements. Using the calculated band parameters, the band diagram of the $\text{Al}_2\text{O}_3/\text{InN}$ heterostructure was calculated as shown in Fig. 8.

In summary, we investigated band alignment between ALD deposited Al_2O_3 and m-plane InN by XPS. The valence band offset and conduction band

offset were determined to be 2.83 eV and 3.17 eV, respectively. A large band offset both in the conduction and valence bands make it a favorable dielectric for future devices. The VBM of InN was found to be 0.63 eV below Fermi level, indicating reduced band bending. The small separation between VBM and E_f provides less carrier concentration near the surface, making the depletion of surface electron easier.

ACKNOWLEDGEMENT

This work was supported by ONR Grant (N000141310214) monitored by Dr. Paul A. Maki and by the Innovative Micro-Programs Accelerating Collaboration in Themes (IMPACT) program funded by the Office of Vice President of Research and Economic Development at the University at Buffalo. A portion of this work was performed in the UB shared instrumentation facility.

REFERENCES

1. J. Wu, W. Walukiewicz, K.M. Yu, J.W. Ager, E.E. Haller, H. Lu, W.J. Schaff, Y. Saito, and Y. Nanishi, *Appl. Phys. Lett.* 80, 21 (2002).
2. T. Matsuoka, H. Okamoto, M. Nakao, H. Harima, and E. Kurimoto, *Appl. Phys. Lett.* 81, 7 (2002).
3. V.YU. Davydov, A.A. Klochikhin, R.P. Seisyan, V.V. Emtsev, S.V. Ivanov, F. Bechstedt, J. Furthmüller, H. Harima, A.V. Mudryi, J. Aderhold, O. Semchinova, and J. Graul, *Phys. Status Solidi B* 229, 3 (2002).
4. P. Carrier and S.-H. Wei, *J. Appl. Phys.* 97, 3 (2005).
5. W.A. Hadi, P.K. Guram, M.S. Shur, and S.K. O'Leary, *J. Appl. Phys.* 113, 11 (2013).
6. K.T. Tsen, C. Poweleit, D.K. Ferry, H. Lu, and W.J. Schaff, *Appl. Phys. Lett.* 86, 22 (2005).
7. V. Lebedev, V. Cimalla, T. Baumann, O. Ambacher, F.M. Morales, J.G. Lozano, and D. González, *J. Appl. Phys.* 100, 9 (2006).
8. H. Lu, W.J. Schaff, L.F. Eastman, and C.E. Stutz, *Appl. Phys. Lett.* 82, 11 (2003).
9. I. Mahboob, T. Veal, C. McConville, H. Lu, and W. Schaff, *Phys. Rev. Lett.* 92, 3 (2004).
10. T.D. Veal, L.F.J. Piper, W.J. Schaff, and C.F. McConville, *J. Cryst. Growth* 288, 2 (2006).
11. S. Choi, F. Wu, O. Bierwagen, and J.S. Speck, *J. Vac. Sci. Technol. A* 31, 3 (2013).
12. S. Li, K. Yu, J. Wu, R. Jones, W. Walukiewicz, J. Ager, W. Shan, E. Haller, H. Lu, and W. Schaff, *Phys. Rev. B* 71, 16 (2005).
13. P.D.C. King, T.D. Veal, P.H. Jefferson, S.A. Hatfield, L.F.J. Piper, C.F. McConville, F. Fuchs, J. Furthmüller, F. Bechstedt, H. Lu, and W.J. Schaff, *Phys. Rev. B* 77, 4 (2008).
14. P.D.C. King, T.D. Veal, and C.F. McConville, *J. Phys. Condens. Matter* 21, 17 (2009).
15. Y.-H. Chang, Y.-S. Lu, Y.-L. Hong, C.-T. Kuo, S. Gwo, and J.A. Yeh, *J. Appl. Phys.* 107, 4 (2010).
16. L.R. Bailey, T.D. Veal, C.E. Kendrick, S.M. Durbin, and C.F. McConville, *Appl. Phys. Lett.* 95, 19 (2009).
17. C.-T. Kuo, S.-C. Lin, K.-K. Chang, H.-W. Shiu, L.-Y. Chang, C.-H. Chen, S.-J. Tang, and S. Gwo, *Appl. Phys. Lett.* 98, 5 (2011).
18. T.D. Veal, P.D.C. King, P.H. Jefferson, L.F.J. Piper, C.F. McConville, H. Lu, W.J. Schaff, P.A. Anderson, S.M. Durbin, D. Muto, H. Naoi, and Y. Nanishi, *Phys. Rev. B* 76, 7 (2007).
19. C.G. Van de Walle and D. Segev, *J. Appl. Phys.* 101, 8 (2007).
20. A. Belabbes, J. Furthmüller, and F. Bechstedt, *Phys. Rev. B* 84, 20 (2011).

21. C.-L. Wu, H.-M. Lee, C.-T. Kuo, C.-H. Chen, and S. Gwo, *Phys. Rev. Lett.* 101, 10 (2008).
22. S. Zhao, S. Fatholouloumi, K.H. Bevan, D.P. Liu, M.G. Kibria, Q. Li, G.T. Wang, H. Guo, and Z. Mi, *Nano Lett.* 12, 6 (2012).
23. S. Zhao, B.H. Le, D.P. Liu, X.D. Liu, M.G. Kibria, T. Szkopek, H. Guo, and Z. Mi, *Nano Lett.* 13, 11 (2013).
24. B.H. Le, S. Zhao, N.H. Tran, T. Szkopek, and Z. Mi, *Appl. Phys. Express* 8, 6 (2015).
25. T. Paskova, *Nitrides with Nonpolar Surfaces: Growth, Properties, and Devices* (Weinheim: Wiley, 2008), p. 23.
26. M.D. Groner, J.W. Elam, F.H. Fabreguette, and S.M. George, *Thin Solid Films* 413, 1 (2002).
27. T.D. Veal, C.F. McConville, and W.J. Schaff, *Indium nitride and related alloys* (Boca Raton: CRC Press, 2010), p. 68.
28. C.-L. Hsiao, J.-T. Chen, H.-C. Hsu, Y.-C. Liao, P.-H. Tseng, Y.-T. Chen, Z.C. Feng, L.-W. Tu, M.M.C. Chou, L.-C. Chen, and K.-H. Chen, *J. Appl. Phys.* 107, 7 (2010).
29. C. Kim, I.K. Robinson, J. Myoung, K. Shim, M.-C. Yoo, and K. Kim, *Appl. Phys. Lett.* 69, 16 (1996).
30. V. Darakchieva, M.Y. Xie, N. Franco, F. Giuliani, B. Nunes, E. Alves, C.L. Hsiao, L.C. Chen, T. Yamaguchi, Y. Takagi, K. Kawashima, and Y. Nanishi, *J. Appl. Phys.* 108, 7 (2010).
31. T.D. Veal, C.F. McConville, and W.J. Schaff, *Indium Nitride and Related Alloys* (Boca Raton: CRC Press, 2011), p. 26.
32. C.J. Lu, L.A. Bendersky, H. Lu, and W.J. Schaff, *Appl. Phys. Lett.* 83, 14 (2003).
33. C.-F. Shih, N.-C. Chen, P.-H. Chang, and K.-S. Liu, *Jpn. J. Appl. Phys.* 44, 11 (2005).
34. T.-H. Hung, K. Sasaki, A. Kuramata, D.N. Nath, P. Sung Park, C. Polchinski, and S. Rajan, *Appl. Phys. Lett.* 104, 16 (2014).
35. E. Kraut, R. Grant, J. Waldrop, and S. Kowalczyk, *Phys. Rev. Lett.* 44, 24 (1980).
36. A. Eisenhardt, G. Eichapfel, M. Himmerlich, A. Knübel, T. Passow, C. Wang, F. Benkhelifa, R. Aidam, and S. Krischok, *Phys. Status Solidi C* 9, 3–4 (2012).
37. P.D.C. King, T.D. Veal, C.E. Kendrick, L.R. Bailey, S.M. Durbin, and C.F. McConville, *Phys. Rev. B* 78, 3 (2008).
38. P.D.C. King, T.D. Veal, P.H. Jefferson, C.F. McConville, T. Wang, P.J. Parbrook, H. Lu, and W.J. Schaff, *Appl. Phys. Lett.* 90, 13 (2007).
39. W.M. Linhart, T.D. Veal, P.D.C. King, G. Koblmüller, C.S. Gallinat, J.S. Speck, and C.F. McConville, *Appl. Phys. Lett.* 97, 11 (2010).
40. S.A. Chambers, T. Droubay, T.C. Kaspar, and M. Gutowski, *J. Vac. Sci. Technol. B* 22, 4 (2004).
41. T. Nagata, G. Koblmüller, O. Bierwagen, C.S. Gallinat, and J.S. Speck, *Appl. Phys. Lett.* 95, 13 (2009).
42. T. Maruyama, K. Yorozu, T. Noguchi, Y. Seki, Y. Saito, T. Araki, and Y. Nanishi, *Phys. Status Solidi C* 7, 2031–2034 (2003).
43. A. Eisenhardt, S. Krischok, and M. Himmerlich, *Appl. Phys. Lett.* 102, 23 (2013).
44. I. Geppert, M. Eizenberg, A. Ali, and S. Datta, *Appl. Phys. Lett.* 97, 16 (2010).
45. S. Miyazaki, *J. Vac. Sci. Technol. B* 19, 6 (2001).
46. M.L. Huang, Y.C. Chang, C.H. Chang, T.D. Lin, J. Kwo, T.B. Wu, and M. Hong, *Appl. Phys. Lett.* 89, 1 (2006).